

DOI: 10.1002/adma.200502364

Integration of Single-Crystal LiNbO₃ Thin Film on Silicon by Laser Irradiation and Ion Implantation–Induced Layer Transfer**

By Young-Bae Park,* Bumki Min, Kerry J. Vahala, and Harry A. Atwater

Ferroelectric materials have found extensive application in microelectronics, microelectromechanical systems (MEMS), and electro-optic devices.^[1] Ferroelectric oxides have been used in modulators, resonators, piezoelectric components, infrared-detector elements, acoustic delay lines, microwave-tunable devices, and in data processing and memory elements. The use of thin-film layers of such ferroelectric oxides can dramatically reduce device operating voltages and enable monolithic device integration. However, the integration of high-quality ferroelectric thin films in planar device architectures on silicon substrates remains a technological challenge. A promising candidate material for such thin-film integration is LiNbO₃, a well-known nonlinear optical crystal that exhibits an extraordinary spontaneous polarization ($71 \mu\text{C cm}^{-2}$). LiNbO₃ optical waveguides are of great importance in electro-optic applications^[2,3] and could be substantially improved through a successful thin-film integration technology.

Direct wafer bonding and layer-transfer techniques are promising methods for fabricating high-quality single-crystal thin films without heteroepitaxial growth and the attendant materials-defect problems associated with lattice mismatch between the thin-film layer and the silicon substrate. Implantation-induced layer transfer processes have previously been reported for the layer transfer of Si, InP, Ge, and diamond.^[4,5] Recently, layer splitting and transfer of ferroelectric materials such as LiNbO₃, LiTaO₃, KTaO₃, SrTiO₃, and BaTiO₃ have also been demonstrated through a sacrificial wet etching and anodic bonding process combined with a crystal ion slicing method.^[6–11] However, because of large mismatch in the coefficient of thermal expansion (CTE) between LiNbO₃ ($(7.5\text{--}14.4) \times 10^{-6} \text{ m }^\circ\text{C}^{-1}$, depending on cutting orientation) and Si ($2.6 \times 10^{-6} \text{ m }^\circ\text{C}^{-1}$), thermal mismatch–induced stress at the LiNbO₃/Si interface occurring during heating and cooling steps in the direct bonding and layer transfer process is quite large in comparison to other material systems. This complicates the development of layer transfer and bonding processes for the integration of LiNbO₃ on silicon.

Laser lift off (LLO) and laser-induced forward transfer methods have been widely investigated as an alternative approach to the integration of PZT (Pb(Zr,Ti)O₃), GaN, and Si thin films. These methods employ excimer laser irradiation and an intermetallic bonding layer (PdIn) as an adhesive layer.^[12–14] However, for the microphotonic device applications anticipated in this study, the LiNbO₃ thin film needs to be formed directly on the silicon substrate without any intermediate metallic adhesive layer.

In this communication, we introduce a novel method of thin-film integration using laser-induced layer transfer in conjunction with ion implantation to integrate single-crystal LiNbO₃ thin films on silicon substrates. Figure 1 represents the overall process. Light ions such as hydrogen and helium are implanted into the single-crystal LiNbO₃ wafer (donor) as shown in Figure 1a. The peak concentration location of ion species can be controlled by the implant energy. An implantation energy of 30 or 80 keV is selected to achieve an expected H⁺ peak concentration approximately 0.2 or 0.8 μm below the donor wafer top surface. The implanted hydrogen and helium ions subsequently introduce microcavities at the peak concentration location during the post-annealing or laser irradiation process steps. The straggle range of the ions is approximately 160 nm for hydrogen, which suggests that the root mean squared (RMS) roughness of the transferred layer is approximately 80 nm. After the implantation, the donor wafer and receptor substrates are cleaned to remove organic contamination and particles and to obtain hydrophilic surfaces, and then bonded at room temperature (Fig. 1b). To induce layer transfer after the bonding step, continuous wave (cw) CO₂ laser irradiation is scanned over the LiNbO₃ wafer, as shown in Fig.

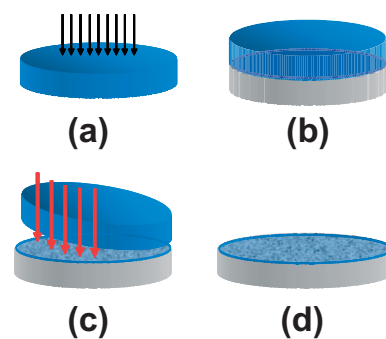


Figure 1. Layer transfer process. a) Ion implantation through donor bulk crystal. b) Wafer bonding process. c) Laser irradiation using $\lambda = 10.6 \mu\text{m}$ CO₂ laser. d) Transferred layer on Si substrate.

[*] Dr. Y.-B. Park, B. Min, Prof. K. J. Vahala, Prof. H. A. Atwater
Thomas J. Watson Laboratories of Applied Physics
California Institute of Technology
MS 128-95, Pasadena, CA 91125 (USA)
E-mail: ypark@caltech.edu

[**] This work has been supported by the Army Research Office (ARO-MURI) under grant no. DAAD 19-01-1-0517 and by Arrowhead Research Corporation.

ure 1c. Thermomechanical shock-induced lateral crack and forward layer transfer are the result, as in the LLO processes.^[12–14] The transferred thickness is consistent with the values predicted using SRIM (Stopping and Range of Ions in Matter, <http://www.srim.org/>) software (Fig. 1d). This implies that most laser power is absorbed in the peak concentration region, where the high-dose implantation (ca. 1×10^{17} ions cm^{-2}) introduces a great deal of damage. The transferred LiNbO_3 thin films have been characterized by optical microscopy (OM), micro-Raman spectroscopy, and atomic force microscopy (AFM)/piezoresponse force microscopy (PFM).

Figure 2a shows a plan-view polarized OM image of the thin-film layers after the laser-induced transfer process. In the transferred LiNbO_3 thin film, one can see cracks along a particular orientation. We have observed similar crack generation in ion-implanted LiNbO_3 bulk crystals that have been irradiated with a CO_2 laser. These observations (Fig. 2b) reveal that cracks form along the domain boundaries with a density of $1.3 \times 10^2 \text{ cm}^{-1}$. It is frequently observed that the intersections between lamellar twin defects act as preferred sites for crack nucleation in bulk LiNbO_3 .^[15,16] This is related to polarization vectors that are arranged head-to-tail along the twin

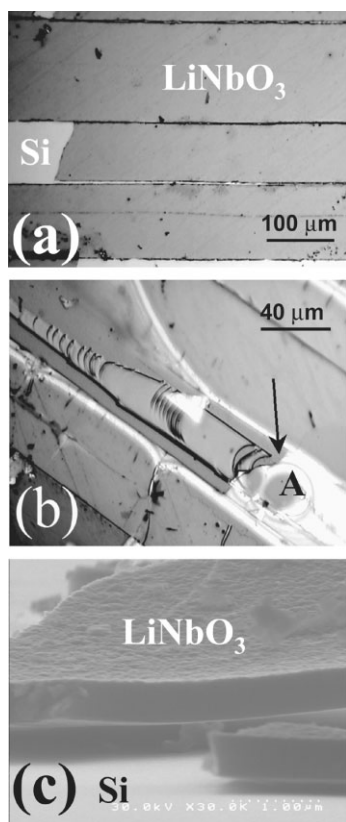


Figure 2. a) Plan-view OM image of transferred LiNbO_3 layer on Si. b) Bulk LiNbO_3 crystal with short-duration laser irradiation on the bulk crystal at the point marked A. c) A layer exfoliated with 500 °C annealing of implanted LiNbO_3 crystal. Implantation energy was 80 keV for the H^+ dose (5×10^{16} ions cm^{-2}) and 115 keV for the He^+ dose (1×10^{17} ions cm^{-2}). Scale bar is 1 μm .

boundary. We speculate that these mechanically cleaved lines are induced by thermal shock during the rapid heating and quenching caused by the laser irradiation and transfer process.^[12] Figure 2c shows an exfoliated thin film bonded to a silicon substrate at 500 °C. Room-temperature bonding resulted in discontinuous and wrinkled transferred thin films, possibly because of lower bond strength associated with room-temperature wafer bonding. In Figure 2c, the thickness of the blister is approximately 800 nm, which is consistent with the Monte Carlo ion trajectory simulation (SRIM-2003) result. Based on the transferred film morphology, we propose that the fundamental mechanism of our layer transfer process is the explosive effusion of the implanted species at the projected ion range. We believe the LiNbO_3 thin film layer is thermomechanically delaminated from the donor LiNbO_3 wafer and transferred to the receptor substrate (Si) during the high-power laser irradiation.

Figure 3 shows AFM and PFM images of the transferred LiNbO_3 layers on a highly doped Si(100) substrate measured at the middle of the transferred area ($34 \mu\text{m} \times 34 \mu\text{m}$). The RMS surface roughness of the LiNbO_3 crystal was increased from 2.0 to 11.0 nm by the high-dose implantation. The RMS roughness of the transferred LiNbO_3 layer is 30.8 nm, owing to the implantation-induced damage at the top of the transferred layer. The increase in RMS roughness is mainly due to the existence of many cavities on the transferred surface, which may be related to Li-evaporation at high temperatures during the rapid heating by the laser.^[4,5] Domain walls were observed through the twin formation from thermal stress during the cooling-down process after layer transfer as seen in Figure 2a. The surface roughness and crystallographic damage will be a critical issue if this transferred LiNbO_3 layer is to be used in an optoelectronic device application. To reduce damage and surface roughness after layer transfer, chemical mechanical polishing processes will be required.

In the piezoresponse image (Fig. 3b), bright and dark areas originate from the downward (positive) and upward (negative) oriented domains, respectively.^[17] Strong dark contrast in domain regions suggests the existence of highly polarized areas even without a poling bias. Figure 3c shows piezoelectric strain versus electric field (P – E) hysteresis curves obtained from the piezoresponse signal (tip amplitude) as a function of dc bias. From the displacement caused by the bias applied between the conducting AFM tip and the substrate, the piezoelectric strain coefficient, d_{33} , can be determined from the equation $\Delta Z = d_{33} V_{\text{ac}} \sin \omega t$, where Z is the longitudinal displacement, V_{ac} the amplitude of the ac voltage, and ω the radial frequency. The piezoelectric strain coefficient in the transferred thin layer was found to be 2.0–2.5 pm V^{-1} , which is smaller than the value obtained for bulk LiNbO_3 (6.0 pm V^{-1}). We believe that this small d_{33} value is due to the clamping effect of the thick Si substrate in the case of the thin film. The piezoelectric strain coefficient may also be improved by a domain poling process step.

LiNbO_3 belongs to the C_{3v} point group ($R3c-3m$) and has four A_1 and nine E Raman-active transitions ($4 A_1 + 9 E$).^[18]

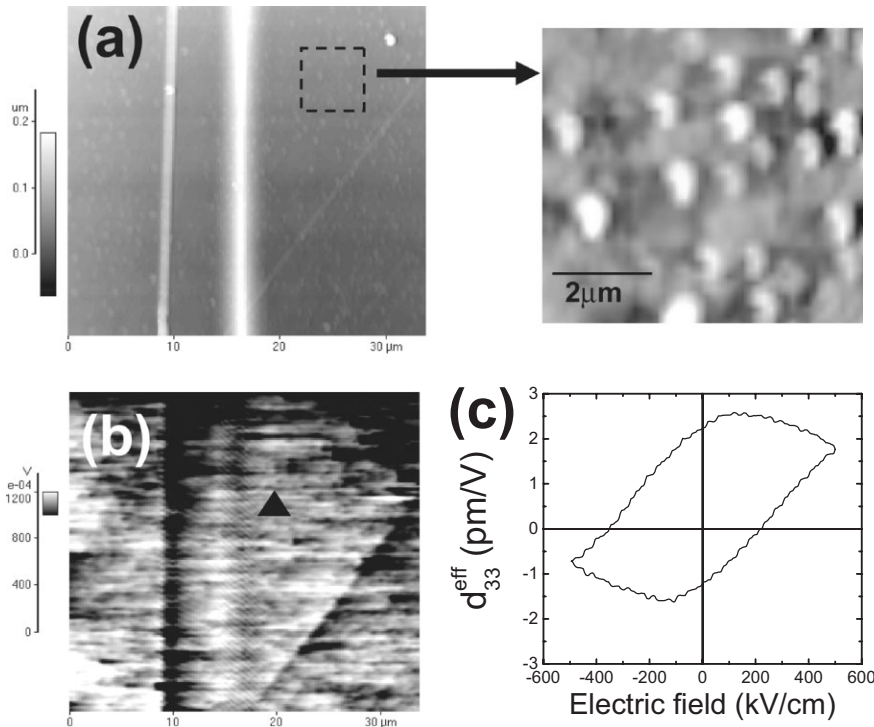


Figure 3. Simultaneously obtained a) AFM topographic image with small scan area image and b) piezoresponse image of the transferred LiNbO₃ layer (200 nm) on the Si. c) Piezoresponse hysteresis (*P*–*E*) curve obtained by piezoresponse signal at the point marked with the black triangle in the domain image in (b). The modulation voltage of the tip, *V*_{ac}, was 1.3 V and modulation frequency was 18 kHz. PFM and AFM images were scanned over a 34 μm × 34 μm area.

In the unprocessed LiNbO₃ (Fig. 4, spectrum a), the bands between 250 and 450 cm⁻¹ are related to Nb–O octahedral

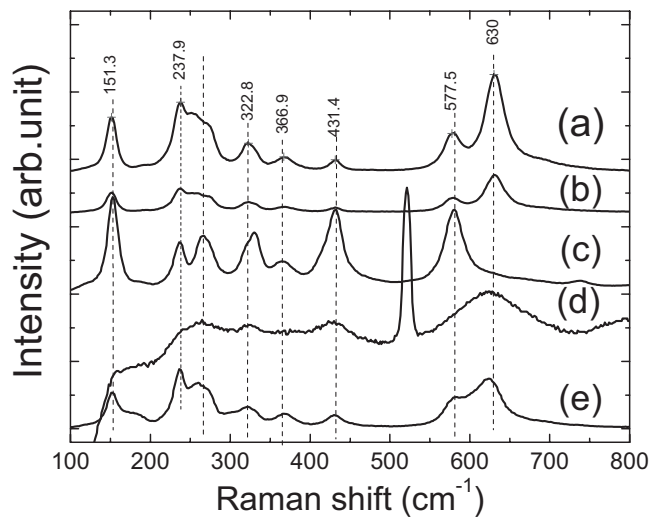


Figure 4. Micro-Raman spectra for a) fresh LiNbO₃ bulk crystal as a reference; b) ion-implanted LiNbO₃, H⁺ dose (80 keV) is 5 × 10¹⁶ ions cm⁻² and He⁺ dose (115 keV) is 1 × 10¹⁷ ions cm⁻²; c) after cw-CO₂ laser irradiation of bulk LiNbO₃; d) the transferred LiNbO₃ on Si (200 nm); and e) transferred LiNbO₃ on Si (800 nm). The strong peak at 520 cm⁻¹ is due to the Si(TO) mode from the Si substrate.

bending modes and the bands from 450 to 800 cm⁻¹ are associated with Nb–O octahedral stretching modes. After the H⁺/He⁺ ion implantation processes, the local modes decrease due to the local damage from the high-dose and high-energy implantation (Fig. 4, spectrum b). The most notable local mode intensity change is in the 250–450 cm⁻¹ band for laser-irradiated LiNbO₃ samples, as shown in Figure 4, spectrum c. This suggests that the niobium octahedra have been distorted or that elemental Li is partially released from the LiNbO₃ structure by laser irradiation. Similar phenomena have been reported in proton-exchanged LiNbO₃ and high-energy He⁺ implantation of LiNbO₃.^[6,19] However, the transferred LiNbO₃ thin films (Fig. 4, spectra d,e) have the same local mode as the original bulk LiNbO₃. These results suggest that the laser-induced thermal energy is primarily confined to the peak implantation concentration region.

Using the transferred LiNbO₃ thin film (800 nm) on Si, we fabricated the micro-disk structure shown in Figure 5. Details of the fabrication process of the micro-disk are given elsewhere.^[20] After

the isotropic dry etch of the Si substrate under the bonded LiNbO₃ using XeF₂, the thin LiNbO₃ layer was observed to shrink, possibly due to strain relaxation during the dry etching. In order to prepare a resonator for communication applications operating at λ = 1.55 μm, the transferred layer thickness will need to be increased in the future. However, considering that much thicker (several micrometer) LiNbO₃ single-crystal films have been reported by Radojevic et al., it should be possible to obtain a moderately thicker film using higher energy (several MeV range) implantation.^[6,7] Izuhara et al.^[7] have also reported freestanding LiNbO₃ layers that are several micrometers thick, suggesting that the transferred LiNbO₃ thickness is ultimately limited by the equipment capability and processing time. Conventional medium-current

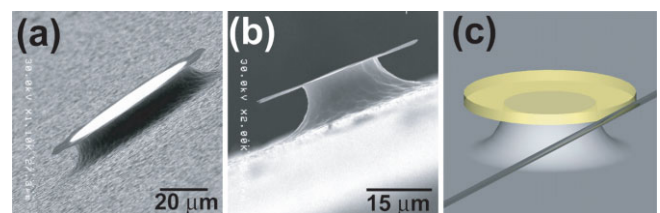


Figure 5. a,b) Secondary electron microscopy images of micro-disk structures using transferred LiNbO₃ thin film on a Si substrate. c) Schematic diagram of a micro-disk in a micro-resonator application [20].

implant equipment commonly employed for achieving the required implantation dose is typically limited to maximum implant energies of around 400 keV, which corresponds to approximately 4.5 μm thick LiNbO_3 thin films. Low-current implant equipment can offer higher implant energies but requires substantially increased processing time, which can be prohibitively expensive. Therefore, a future goal of this study will be epitaxial growth on the transferred single-crystal LiNbO_3 to increase the film thickness. The LiNbO_3 thin-film template layer will be essential in this process as epitaxial growth directly on a Si surface is difficult due to the huge lattice constant and CTE mismatch between Si and LiNbO_3 .^[21] The thin-film thicknesses achieved in this study are sufficient for these future applications of transferred LiNbO_3 as template layers for epitaxial growth, provided that the damage of the top layer in the transferred thin film can be removed.

In conclusion, we have investigated a novel fabrication process for the integration of single-crystal LiNbO_3 thin films on silicon using a combination of wafer bonding and layer transfer induced by laser irradiation in conjunction with ion implantation. High-dose and high-energy H^+ and He^+ co-implantation is used to synthesize a buried damage layer in the LiNbO_3 bulk crystal, which is bonded to the Si substrate. After bonding, high power cw- CO_2 laser-irradiation is used to induce the formation and lateral propagation of gas microcavities at the buried damage layer through the rapid absorption of radiation heat, eventually leading to localized layer exfoliation from the LiNbO_3 donor substrate. Large-area single-crystal LiNbO_3 thin films (6 mm^2 , 200–800 nm thick) have been transferred to the Si(100) substrates and exhibit typical piezoelectric characteristics. A suspended micro-disk resonator structure has been successfully fabricated, suggesting that our fabrication approach may be useful in optoelectronic device applications. The thin LiNbO_3 layer transferred to the Si wafer may additionally serve as a template layer for subsequent thick LiNbO_3 growth. This templated growth process may be more feasible for commercial application in consideration of the cost of high-energy ion implantation.

Experimental

Layer Transfer Processes: To achieve implantation-induced layer transfer, ion implantation was performed with H^+ and He^+ co-implantation into bulk single-crystal LiNbO_3 (double side polished, z-cut, 10 mm \times 10 mm \times 0.5 mm) as shown in Figure 1a. During the implantation, LiNbO_3 crystals were placed on 4 inch (ca. 10 cm) Si wafer. The ion implantation energy was 20–80 keV with a dose of $(0.5\text{--}1) \times 10^{17} \text{ cm}^{-2}$ for the H^+ ions and 30–115 keV with a dose of $(0.5\text{--}1) \times 10^{17} \text{ cm}^{-2}$ for the He^+ ions. Implantation was performed at 25 °C to prevent blistering during implantation. The substrate used for bonding and layer transfer was a highly doped n-Si(100) wafer with RMS surface roughness of 0.2 nm. Prior to the layer transfer process, acetone (5 min)/ methanol (5 min)/deionized water (10 min) dipping was repeatedly performed to remove particles from the surface. After this cleaning process, the Si wafer and LiNbO_3 crystal were bonded at room temperature and at 500 °C without HF dipping in or-

der to preserve hydrophilic surface conditions. Wafer bonding was performed under uniaxial pressure of 1–2 MPa using a custom wafer bonding tool.

High power cw- CO_2 laser (100 MW m^{-2}) irradiation was used as a heat source to induce layer transfer instead of thermal annealing. Under the fixed laser power, the sample stage was scanned across the bonding area. The bonded LiNbO_3 crystal/Si substrate was clamped to the translation stage by a clip at the edge of the layer.

Characterization: Polarized optical microscopy, secondary electron microscopy, and AFM were used to image the transferred layer. Micro-Raman spectroscopy measurements were made using 514.5 nm Ar^+ laser excitation and imaging with a charge-coupled device camera cooled to -65°C . Laser power was maintained at 16 mW cm^{-2} to avoid surface heating during the measurement. PFM and contact-mode AFM were used to investigate the ferroelectric domain structure using a lock-in amplifier (Stanford Research Model SR-850). An ac voltage, $V_{\text{ac}} = 1.5 \text{ V}$, was applied at a frequency of 1.5–10 kHz through the conductive AFM tip (highly n-doped Si or Co-coated Si), while the dc bias voltage was varied between -10 and $+10 \text{ V}$ [17].

Micro-disk Fabrication: Conventional photolithography was used to define the LiNbO_3 micro-disk. After photoresist had been patterned on the transferred LiNbO_3 layer, a buffered HF (1:10) solution was used to etch LiNbO_3 . The suspended micro-disk was defined by XeF_2 etching of the Si using the LiNbO_3 layer as a mask. XeF_2 selectively etches Si over the LiNbO_3 disk. More details of the fabrication process are given elsewhere [20].

Received: November 3, 2005

Final version: April 4, 2006

Published online: May 18, 2006

- [1] A. I. Kingon, J. P. Maria, S. K. Streiffer, *Nature* **2000**, 406, 1032.
- [2] R. S. Weis, T. K. Gaylord, *Appl. Phys. A* **1985**, 37, 191.
- [3] A. M. Radojevic, R. M. Osgood, M. Levy, A. Kumar, H. Bakhr, *IEEE Photon. Technol. Lett.* **2000**, 12, 1653.
- [4] M. Bruel, *Electron. Lett.* **1995**, 31, 1201.
- [5] Q.-Y. Tong, K. Gutjahr, S. Hopfe, U. Gösele, T.-H. Lee, *Appl. Phys. Lett.* **1997**, 70, 1390.
- [6] A. M. Radojevic, M. Levy, R. M. Osgood, A. Kumar, H. Bakhr, C. Tian, C. Evans, *Appl. Phys. Lett.* **1999**, 74, 3197.
- [7] T. Izuhara, R. M. Osgood, M. Levy, M. E. Reeves, Y. G. Wang, A. N. Roy, H. Bakhr, *Appl. Phys. Lett.* **2002**, 80, 1046.
- [8] A. Namba, M. Sugimoto, T. Ogura, Y. Tomita, K. Eda, *Appl. Phys. Lett.* **1995**, 67, 3275.
- [9] I. Radu, I. Szafraniak, R. Scholz, M. Alexe, U. Gösele, *Integ. Ferroelectr.* **2003**, 55, 983.
- [10] T. Izuhara, I. Gheorma, R. M. Osgood, A. N. Roy, H. Bakhr, Y. M. Tesfu, M. E. Reeves, *Appl. Phys. Lett.* **2003**, 82, 616.
- [11] Y.-B. Park, J. Ruglovsky, H. A. Atwater, *Appl. Phys. Lett.* **2004**, 85, 455.
- [12] L. Tsakalagos, T. Sands, *Appl. Phys. Lett.* **2000**, 76, 227.
- [13] P. R. Tavernier, D. R. Clarke, *J. Appl. Phys.* **2001**, 89, 1527.
- [14] D. Toet, M. O. Thomson, P. M. Smith, T. W. Sigmon, *Appl. Phys. Lett.* **1999**, 74, 2170.
- [15] B. M. Park, K. Kitamura, Y. Furukawa, Y. Ji, *J. Am. Ceram. Soc.* **1997**, 80, 2689.
- [16] A. W. Vere, *J. Mater. Sci.* **1968**, 3, 617.
- [17] A. Gruverman, O. Auciello, H. Tokumoto, *Annu. Rev. Mater. Sci.* **1998**, 28, 101.
- [18] J. Jehng, I. E. Wachs, *Chem. Mater.* **1991**, 3, 100.
- [19] G. R. Pa-Pujalt, D. D. Tuschel, *Appl. Phys. Lett.* **1993**, 62, 3411.
- [20] D. Armani, B. Min, A. Martin, K. J. Vahala, *Appl. Phys. Lett.* **2004**, 85, 5439.
- [21] V. A. Joshkin, P. Moran, D. Saulys, T. F. Kuech, L. McCaughan, S. R. Oktyabrsky, *Appl. Phys. Lett.* **2000**, 76, 2125.